

Measurement of Time-Dependent CP Asymmetries and Constraints on $\sin(2\beta + \gamma)$ with Partial Reconstruction of $B^0 \rightarrow D^{*\mp} \pi^\pm$ Decays

The *BABAR* Collaboration

October 28, 2018

Abstract

We present a preliminary measurement of the time-dependent CP -violating asymmetry in decays of neutral B mesons to the final states $D^{*\mp} \pi^\pm$, using approximately 178 million $B\bar{B}$ events recorded by the *BABAR* experiment at the PEP-II e^+e^- storage ring. Events containing these decays are selected with a partial reconstruction technique, in which only the high-momentum π^\pm from the B decay and the low-momentum π^\mp from the $D^{*\mp}$ decay are used. We measure the amplitude of the asymmetry to be -0.041 ± 0.016 (*stat.*) ± 0.010 (*syst.*) and determine bounds on $|\sin(2\beta + \gamma)|$.

Submitted to the 32nd International Conference on High-Energy Physics, ICHEP 04,
16 August—22 August 2004, Beijing, China

Stanford Linear Accelerator Center, Stanford University, Stanford, CA 94309

Work supported in part by Department of Energy contract DE-AC03-76SF00515.

The BABAR Collaboration,

B. Aubert, R. Barate, D. Boutigny, F. Couderc, J.-M. Gaillard, A. Hicheur, Y. Karyotakis, J. P. Lees,
V. Tisserand, A. Zghiche

Laboratoire de Physique des Particules, F-74941 Annecy-le-Vieux, France

A. Palano, A. Pompili

Università di Bari, Dipartimento di Fisica and INFN, I-70126 Bari, Italy

J. C. Chen, N. D. Qi, G. Rong, P. Wang, Y. S. Zhu

Institute of High Energy Physics, Beijing 100039, China

G. Eigen, I. Ofte, B. Stugu

University of Bergen, Inst. of Physics, N-5007 Bergen, Norway

G. S. Abrams, A. W. Borgland, A. B. Breon, D. N. Brown, J. Button-Shafer, R. N. Cahn, E. Charles,
C. T. Day, M. S. Gill, A. V. Gritsan, Y. Groysman, R. G. Jacobsen, R. W. Kadel, J. Kadyk, L. T. Kerth,
Yu. G. Kolomensky, G. Kukartsev, G. Lynch, L. M. Mir, P. J. Oddone, T. J. Orimoto, M. Pripstein,
N. A. Roe, M. T. Ronan, V. G. Shelkov, W. A. Wenzel

Lawrence Berkeley National Laboratory and University of California, Berkeley, CA 94720, USA

M. Barrett, K. E. Ford, T. J. Harrison, A. J. Hart, C. M. Hawkes, S. E. Morgan, A. T. Watson

University of Birmingham, Birmingham, B15 2TT, United Kingdom

M. Fritsch, K. Goetzen, T. Held, H. Koch, B. Lewandowski, M. Pelizaeus, M. Steinke
Ruhr Universität Bochum, Institut für Experimentalphysik 1, D-44780 Bochum, Germany

J. T. Boyd, N. Chevalier, W. N. Cottingham, M. P. Kelly, T. E. Latham, F. F. Wilson

University of Bristol, Bristol BS8 1TL, United Kingdom

T. Cuhadar-Donszelmann, C. Hearty, N. S. Knecht, T. S. Mattison, J. A. McKenna, D. Thiessen

University of British Columbia, Vancouver, BC, Canada V6T 1Z1

A. Khan, P. Kyberd, L. Teodorescu

Brunel University, Uxbridge, Middlesex UB8 3PH, United Kingdom

A. E. Blinov, V. E. Blinov, V. P. Druzhinin, V. B. Golubev, V. N. Ivanchenko, E. A. Kravchenko,
A. P. Onuchin, S. I. Serebnyakov, Yu. I. Skovpen, E. P. Solodov, A. N. Yushkov

Budker Institute of Nuclear Physics, Novosibirsk 630090, Russia

D. Best, M. Bruinsma, M. Chao, I. Eschrich, D. Kirkby, A. J. Lankford, M. Mandelkern, R. K. Mommsen,
W. Roethel, D. P. Stoker

University of California at Irvine, Irvine, CA 92697, USA

C. Buchanan, B. L. Hartfiel

University of California at Los Angeles, Los Angeles, CA 90024, USA

S. D. Foulkes, J. W. Gary, B. C. Shen, K. Wang

University of California at Riverside, Riverside, CA 92521, USA

- D. del Re, H. K. Hadavand, E. J. Hill, D. B. MacFarlane, H. P. Paar, Sh. Rahatlou, V. Sharma
University of California at San Diego, La Jolla, CA 92093, USA
- J. W. Berryhill, C. Campagnari, B. Dahmes, O. Long, A. Lu, M. A. Mazur, J. D. Richman, W. Verkerke
University of California at Santa Barbara, Santa Barbara, CA 93106, USA
- T. W. Beck, A. M. Eisner, C. A. Heusch, J. Kroseberg, W. S. Lockman, G. Nesom, T. Schalk,
B. A. Schumm, A. Seiden, P. Spradlin, D. C. Williams, M. G. Wilson
University of California at Santa Cruz, Institute for Particle Physics, Santa Cruz, CA 95064, USA
- J. Albert, E. Chen, G. P. Dubois-Felsmann, A. Dvoretzki, D. G. Hitlin, I. Narsky, T. Piatenko,
F. C. Porter, A. Ryd, A. Samuel, S. Yang
California Institute of Technology, Pasadena, CA 91125, USA
- S. Jayatileke, G. Mancinelli, B. T. Meadows, M. D. Sokoloff
University of Cincinnati, Cincinnati, OH 45221, USA
- T. Abe, F. Blanc, P. Bloom, S. Chen, W. T. Ford, U. Nauenberg, A. Olivas, P. Rankin, J. G. Smith,
J. Zhang, L. Zhang
University of Colorado, Boulder, CO 80309, USA
- A. Chen, J. L. Harton, A. Soffer, W. H. Toki, R. J. Wilson, Q. L. Zeng
Colorado State University, Fort Collins, CO 80523, USA
- D. Altenburg, T. Brandt, J. Brose, M. Dickopp, E. Feltresi, A. Hauke, H. M. Lacker, R. Müller-Pfefferkorn,
R. Nogowski, S. Otto, A. Petzold, J. Schubert, K. R. Schubert, R. Schwierz, B. Spaan, J. E. Sundermann
Technische Universität Dresden, Institut für Kern- und Teilchenphysik, D-01062 Dresden, Germany
- D. Bernard, G. R. Bonneaud, F. Brochard, P. Grenier, S. Schrenk, Ch. Thiebaux, G. Vasileiadis, M. Verderi
Ecole Polytechnique, LLR, F-91128 Palaiseau, France
- D. J. Bard, P. J. Clark, D. Lavin, F. Muheim, S. Playfer, Y. Xie
University of Edinburgh, Edinburgh EH9 3JZ, United Kingdom
- M. Andreotti, V. Azzolini, D. Bettoni, C. Bozzi, R. Calabrese, G. Cibinetto, E. Luppi, M. Negrini,
L. Piemontese, A. Sarti
Università di Ferrara, Dipartimento di Fisica and INFN, I-44100 Ferrara, Italy
- E. Treadwell
Florida A&M University, Tallahassee, FL 32307, USA
- F. Anulli, R. Baldini-Ferrolì, A. Calcaterra, R. de Sangro, G. Finocchiaro, P. Patteri, I. M. Peruzzi,
M. Piccolo, A. Zallo
Laboratori Nazionali di Frascati dell'INFN, I-00044 Frascati, Italy
- A. Buzzo, R. Capra, R. Contri, G. Crosetti, M. Lo Vetere, M. Macri, M. R. Monge, S. Passaggio,
C. Patrignani, E. Robutti, A. Santroni, S. Tosi
Università di Genova, Dipartimento di Fisica and INFN, I-16146 Genova, Italy
- S. Bailey, G. Brandenburg, K. S. Chaisanguanthum, M. Morii, E. Won
Harvard University, Cambridge, MA 02138, USA

R. S. Dubitzky, U. Langenegger

Universität Heidelberg, Physikalisches Institut, Philosophenweg 12, D-69120 Heidelberg, Germany

W. Bhimji, D. A. Bowerman, P. D. Dauncey, U. Egede, J. R. Gaillard, G. W. Morton, J. A. Nash,
M. B. Nikolich, G. P. Taylor

Imperial College London, London, SW7 2AZ, United Kingdom

M. J. Charles, G. J. Grenier, U. Mallik

University of Iowa, Iowa City, IA 52242, USA

J. Cochran, H. B. Crawley, J. Lamsa, W. T. Meyer, S. Prell, E. I. Rosenberg, A. E. Rubin, J. Yi

Iowa State University, Ames, IA 50011-3160, USA

M. Biasini, R. Covarelli, M. Pioppi

Università di Perugia, Dipartimento di Fisica and INFN, I-06100 Perugia, Italy

M. Davier, X. Giroux, G. Grosdidier, A. Höcker, S. Laplace, F. Le Diberder, V. Lepeltier, A. M. Lutz,
T. C. Petersen, S. Plaszczynski, M. H. Schune, L. Tantot, G. Wormser

Laboratoire de l'Accélérateur Linéaire, F-91898 Orsay, France

C. H. Cheng, D. J. Lange, M. C. Simani, D. M. Wright

Lawrence Livermore National Laboratory, Livermore, CA 94550, USA

A. J. Bevan, C. A. Chavez, J. P. Coleman, I. J. Forster, J. R. Fry, E. Gabathuler, R. Gamet,
D. E. Hutchcroft, R. J. Parry, D. J. Payne, R. J. Sloane, C. Touramanis

University of Liverpool, Liverpool L69 7ZE, United Kingdom

J. J. Back,¹ C. M. Cormack, P. F. Harrison,¹ F. Di Lodovico, G. B. Mohanty¹

Queen Mary, University of London, E1 4NS, United Kingdom

C. L. Brown, G. Cowan, R. L. Flack, H. U. Flaecher, M. G. Green, P. S. Jackson, T. R. McMahon,
S. Ricciardi, F. Salvatore, M. A. Winter

*University of London, Royal Holloway and Bedford New College, Egham, Surrey TW20 0EX,
United Kingdom*

D. Brown, C. L. Davis

University of Louisville, Louisville, KY 40292, USA

J. Allison, N. R. Barlow, R. J. Barlow, P. A. Hart, M. C. Hodgkinson, G. D. Lafferty, A. J. Lyon,
J. C. Williams

University of Manchester, Manchester M13 9PL, United Kingdom

A. Farbin, W. D. Hulsbergen, A. Jawahery, D. Kovalskyi, C. K. Lae, V. Lillard, D. A. Roberts

University of Maryland, College Park, MD 20742, USA

G. Blaylock, C. Dallapiccola, K. T. Flood, S. S. Hertzbach, R. Kofler, V. B. Koptchev, T. B. Moore,
S. Saremi, H. Staengle, S. Willocq

University of Massachusetts, Amherst, MA 01003, USA

¹Now at Department of Physics, University of Warwick, Coventry, United Kingdom

R. Cowan, G. Sciolla, S. J. Sekula, F. Taylor, R. K. Yamamoto
Massachusetts Institute of Technology, Laboratory for Nuclear Science, Cambridge, MA 02139, USA

D. J. J. Mangeol, P. M. Patel, S. H. Robertson
McGill University, Montréal, QC, Canada H3A 2T8

A. Lazzaro, V. Lombardo, F. Palombo
Università di Milano, Dipartimento di Fisica and INFN, I-20133 Milano, Italy

J. M. Bauer, L. Cremaldi, V. Eschenburg, R. Godang, R. Kroeger, J. Reidy, D. A. Sanders, D. J. Summers,
H. W. Zhao
University of Mississippi, University, MS 38677, USA

S. Brunet, D. Côté, P. Taras
Université de Montréal, Laboratoire René J. A. Lévesque, Montréal, QC, Canada H3C 3J7

H. Nicholson
Mount Holyoke College, South Hadley, MA 01075, USA

N. Cavallo, F. Fabozzi,² C. Gatto, L. Lista, D. Monorchio, P. Paolucci, D. Piccolo, C. Sciacca
Università di Napoli Federico II, Dipartimento di Scienze Fisiche and INFN, I-80126, Napoli, Italy

M. Baak, H. Bulten, G. Raven, H. L. Snoek, L. Wilden
*NIKHEF, National Institute for Nuclear Physics and High Energy Physics, NL-1009 DB Amsterdam,
The Netherlands*

C. P. Jessop, J. M. LoSecco
University of Notre Dame, Notre Dame, IN 46556, USA

T. Allmendinger, K. K. Gan, K. Honscheid, D. Hufnagel, H. Kagan, R. Kass, T. Pulliam, A. M. Rahimi,
R. Ter-Antonyan, Q. K. Wong
Ohio State University, Columbus, OH 43210, USA

J. Brau, R. Frey, O. Igonkina, C. T. Potter, N. B. Sinev, D. Strom, E. Torrence
University of Oregon, Eugene, OR 97403, USA

F. Colecchia, A. Dorigo, F. Galeazzi, M. Margoni, M. Morandin, M. Posocco, M. Rotondo, F. Simonetto,
R. Stroili, G. Tiozzo, C. Voci
Università di Padova, Dipartimento di Fisica and INFN, I-35131 Padova, Italy

M. Benayoun, H. Briand, J. Chauveau, P. David, Ch. de la Vaissière, L. Del Buono, O. Hamon,
M. J. J. John, Ph. Leruste, J. Malcles, J. Ocariz, M. Pivk, L. Roos, S. T'Jampens, G. Therin
*Universités Paris VI et VII, Laboratoire de Physique Nucléaire et de Hautes Energies, F-75252 Paris,
France*

P. F. Manfredi, V. Re
Università di Pavia, Dipartimento di Elettronica and INFN, I-27100 Pavia, Italy

²Also with Università della Basilicata, Potenza, Italy

P. K. Behera, L. Gladney, Q. H. Guo, J. Panetta
University of Pennsylvania, Philadelphia, PA 19104, USA

C. Angelini, G. Batignani, S. Bettarini, M. Bondioli, F. Bucci, G. Calderini, M. Carpinelli, F. Forti,
M. A. Giorgi, A. Lusiani, G. Marchiori, F. Martinez-Vidal,³ M. Morganti, N. Neri, E. Paoloni, M. Rama,
G. Rizzo, F. Sandrelli, J. Walsh
Università di Pisa, Dipartimento di Fisica, Scuola Normale Superiore and INFN, I-56127 Pisa, Italy

M. Haire, D. Judd, K. Paick, D. E. Wagoner
Prairie View A&M University, Prairie View, TX 77446, USA

N. Danielson, P. Elmer, Y. P. Lau, C. Lu, V. Miftakov, J. Olsen, A. J. S. Smith, A. V. Telnov
Princeton University, Princeton, NJ 08544, USA

F. Bellini, G. Cavoto,⁴ R. Faccini, F. Ferrarotto, F. Ferroni, M. Gaspero, L. Li Gioi, M. A. Mazzoni,
S. Morganti, M. Pierini, G. Piredda, F. Safai Tehrani, C. Voena
Università di Roma La Sapienza, Dipartimento di Fisica and INFN, I-00185 Roma, Italy

S. Christ, G. Wagner, R. Waldi
Universität Rostock, D-18051 Rostock, Germany

T. Adye, N. De Groot, B. Franek, N. I. Geddes, G. P. Gopal, E. O. Olaiya
Rutherford Appleton Laboratory, Chilton, Didcot, Oxon, OX11 0QX, United Kingdom

R. Aleksan, S. Emery, A. Gaidot, S. F. Ganzhur, P.-F. Giraud, G. Hamel de Monchenault, W. Kozanecki,
M. Legendre, G. W. London, B. Mayer, G. Schott, G. Vasseur, Ch. Yèche, M. Zito
DSM/Daphnia, CEA/Saclay, F-91191 Gif-sur-Yvette, France

M. V. Purohit, A. W. Weidemann, J. R. Wilson, F. X. Yumiceva
University of South Carolina, Columbia, SC 29208, USA

D. Aston, R. Bartoldus, N. Berger, A. M. Boyarski, O. L. Buchmueller, R. Claus, M. R. Convery,
M. Cristinziani, G. De Nardo, D. Dong, J. Dorfan, D. Dujmic, W. Dunwoodie, E. E. Elsen, S. Fan,
R. C. Field, T. Glanzman, S. J. Gowdy, T. Hadig, V. Halyo, C. Hast, T. Hryn'ova, W. R. Innes,
M. H. Kelsey, P. Kim, M. L. Kocian, D. W. G. S. Leith, J. Libby, S. Luitz, V. Luth, H. L. Lynch,
H. Marsiske, R. Messner, D. R. Muller, C. P. O'Grady, V. E. Ozcan, A. Perazzo, M. Perl, S. Petrak,
B. N. Ratcliff, A. Roodman, A. A. Salnikov, R. H. Schindler, J. Schwiening, G. Simi, A. Snyder, A. Soha,
J. Stelzer, D. Su, M. K. Sullivan, J. Va'vra, S. R. Wagner, M. Weaver, A. J. R. Weinstein,
W. J. Wisniewski, M. Wittgen, D. H. Wright, A. K. Yarritu, C. C. Young
Stanford Linear Accelerator Center, Stanford, CA 94309, USA

P. R. Burchat, A. J. Edwards, T. I. Meyer, B. A. Petersen, C. Roat
Stanford University, Stanford, CA 94305-4060, USA

S. Ahmed, M. S. Alam, J. A. Ernst, M. A. Saeed, M. Saleem, F. R. Wappler
State University of New York, Albany, NY 12222, USA

³Also with IFIC, Instituto de Física Corpuscular, CSIC-Universidad de Valencia, Valencia, Spain

⁴Also with Princeton University, Princeton, USA

W. Bugg, M. Krishnamurthy, S. M. Spanier
University of Tennessee, Knoxville, TN 37996, USA

R. Eckmann, H. Kim, J. L. Ritchie, A. Satpathy, R. F. Schwitters
University of Texas at Austin, Austin, TX 78712, USA

J. M. Izen, I. Kitayama, X. C. Lou, S. Ye
University of Texas at Dallas, Richardson, TX 75083, USA

F. Bianchi, M. Bona, F. Gallo, D. Gamba
Università di Torino, Dipartimento di Fisica Sperimentale and INFN, I-10125 Torino, Italy

L. Bosisio, C. Cartaro, F. Cossutti, G. Della Ricca, S. Dittongo, S. Grancagnolo, L. Lanceri, P. Poropat,⁵
L. Vitale, G. Vuagnin
Università di Trieste, Dipartimento di Fisica and INFN, I-34127 Trieste, Italy

R. S. Panvini
Vanderbilt University, Nashville, TN 37235, USA

Sw. Banerjee, C. M. Brown, D. Fortin, P. D. Jackson, R. Kowalewski, J. M. Roney, R. J. Sobie
University of Victoria, Victoria, BC, Canada V8W 3P6

H. R. Band, B. Cheng, S. Dasu, M. Datta, A. M. Eichenbaum, M. Graham, J. J. Hollar, J. R. Johnson,
P. E. Kutter, H. Li, R. Liu, A. Mihalyi, A. K. Mohapatra, Y. Pan, R. Prepost, P. Tan, J. H. von
Wimmersperg-Toeller, J. Wu, S. L. Wu, Z. Yu
University of Wisconsin, Madison, WI 53706, USA

M. G. Greene, H. Neal
Yale University, New Haven, CT 06511, USA

⁵Deceased

1 INTRODUCTION

The Cabibbo-Kobayashi-Maskawa (CKM) quark-mixing matrix [1] gives an explanation of CP violation and is under experimental investigation aimed at constraining its parameters. A crucial part of this program is the measurement of the angle $\gamma = \arg(-V_{ud}V_{ub}^*/V_{cd}V_{cb}^*)$ of the unitarity triangle related to the CKM matrix. The decay modes $B^0 \rightarrow D^{*\mp}\pi^\pm$ have been proposed for use in measurements of $\sin(2\beta + \gamma)$ [2], where $\beta = \arg(-V_{cd}V_{cb}^*/V_{td}V_{tb}^*)$ is well measured [3]. In the Standard Model the decays $B^0 \rightarrow D^{*+}\pi^-$ and $\bar{B}^0 \rightarrow D^{*+}\pi^-$ proceed through the $\bar{b} \rightarrow \bar{u}c\bar{d}$ and $b \rightarrow c\bar{u}d$ amplitudes A_u and A_c . The relative weak phase between the two amplitudes in the usual Wolfenstein convention [4] is γ . When combined with $B^0\bar{B}^0$ mixing, this yields a weak phase difference of $2\beta + \gamma$ between the interfering amplitudes.

The decay rate distribution for $B \rightarrow D^{*\pm}\pi^\mp$ is

$$P_\eta^\pm(\Delta t) = \frac{e^{-|\Delta t|/\tau}}{4\tau} \times \left[1 \mp S^\zeta \sin(\Delta m \Delta t) \mp \eta C \cos(\Delta m \Delta t) \right], \quad (1)$$

where τ is the B^0 lifetime averaged over the two mass eigenstates, Δm is the $B^0 - \bar{B}^0$ mixing frequency, and Δt is the difference between the time of the $B \rightarrow D^{*\pm}\pi^\mp$ (B_{rec}) decay and the decay of the other B (B_{tag}) in the event. The upper (lower) sign in Eq. (1) indicates the flavor of the B_{tag} as a B^0 (\bar{B}^0), while $\eta = +1$ (-1) and $\zeta = +$ ($-$) for the B_{rec} final state $D^{*-}\pi^+$ ($D^{*+}\pi^-$). The parameters C and S^\pm are given by

$$C \equiv \frac{1 - r_{D^{*}\pi}^2}{1 + r_{D^{*}\pi}^2}, \quad S^\pm \equiv \frac{2r_{D^{*}\pi}}{1 + r_{D^{*}\pi}^2} \sin(2\beta + \gamma \pm \delta_{D^{*}\pi}). \quad (2)$$

Here $\delta_{D^{*}\pi}$ is the strong phase difference between A_u and A_c and $r_{D^{*}\pi} = |A_u/A_c|$. Since A_u is doubly CKM-suppressed with respect to A_c , one expects $r_{D^{*}\pi} \sim 0.02$.

We report a study of the CP -violating asymmetry in $B^0 \rightarrow D^{*\mp}\pi^\pm$ decays using the technique of partial reconstruction, which allows us to analyze a large sample of signal events. We use approximately twice the integrated luminosity used in our previous analysis of this process [5], and employ an improved method to eliminate a measurement bias, as described in Sec. 3.4.2.

2 THE BABAR DETECTOR AND DATASET

The data used in this analysis were recorded with the *BABAR* detector at the PEP-II storage ring, and consist of 165.6 fb^{-1} collected on the $\Upsilon(4S)$ resonance (on-resonance sample), and 16 fb^{-1} collected at an e^+e^- CM energy approximately 40 MeV below the resonance peak (off-resonance sample). Samples of simulated Monte Carlo (MC) events with an equivalent luminosity 4 times larger than the data are analyzed through the same analysis procedure.

The *BABAR* detector is described in detail in Ref. [8]. We provide a brief description of the main components and their use in this analysis. Charged-particle trajectories are measured by a combination of a five-layer silicon vertex tracker (SVT) and a 40-layer drift chamber (DCH) in a 1.5 T solenoidal magnetic field. Tracks with low transverse momentum can be reconstructed in the SVT alone, thus extending the charged-particle detection down to transverse momenta of about 50 MeV/c. We use a ring-imaging Cherenkov detector (DIRC) for charged-particle identification and augment it with energy-loss measurements from the SVT and DCH. Photons and electrons are detected in a CsI(Tl) electromagnetic calorimeter (EMC), with photon-energy resolution $\sigma_E/E = 0.023(E/\text{GeV})^{-1/4} \oplus 0.019$. The instrumented flux return (IFR) is equipped with resistive plate chambers to identify muons.

3 ANALYSIS METHOD

3.1 PARTIAL RECONSTRUCTION OF $B^0 \rightarrow D^{*\mp}\pi^\pm$

In the partial reconstruction of a $B^0 \rightarrow D^{*\mp}\pi^\pm$ candidate (B_{rec}), only the hard (high-momentum) pion track π_h from the B decay and the soft (low-momentum) pion track π_s from the decay $D^{*-} \rightarrow \bar{D}^0\pi_s^-$ are used. Applying kinematic constraints consistent with the signal decay mode, we calculate the four-momentum of the unreconstructed, “missing” D , obtaining its flight direction to within a few degrees and its invariant mass m_{miss} [6]. Signal events peak in the m_{miss} distribution at the nominal D^0 mass M_{D^0} with an r.m.s. of 3 MeV/ c^2 (Fig. 1).

3.2 BACKGROUNDS

In addition to $B^0 \rightarrow D^{*\mp}\pi^\pm$ events, the selected event sample contains the following kinds of events: $B \rightarrow D^{*\mp}\rho^\pm$; $B\bar{B}$ background peaking in m_{miss} , composed of pairs of tracks coming from the same B meson, with the π_s originating from a charged D^* decay, excluding $B \rightarrow D^{*\mp}\rho^\pm$ decays; combinatoric $B\bar{B}$ background, defined as all remaining $B\bar{B}$ background events; and continuum $e^+e^- \rightarrow q\bar{q}$, where q represents a u , d , s , or c quark. We suppress the combinatoric background with selection criteria based on the event shape and the D^* helicity-angle. We reject π_h candidates that are identified as leptons or kaons. All candidates must satisfy the requirement $1.81 < m_{\text{miss}} < 1.88$ GeV/ c^2 . Multiple candidates are found in 5% of the events. In these instances, only the candidate with the m_{miss} value closest to M_{D^0} is used.

3.3 DECAY TIME MEASUREMENT AND FLAVOR TAGGING

To perform this analysis, Δt and the flavor of the B_{tag} must be determined. We tag the flavor of the B_{tag} using lepton or kaon candidates. The lepton CM momentum is required to be greater than 1.1 GeV/ c to suppress “cascade” leptons that originate from charm decays. If several flavor-tagging tracks are present in either the lepton or kaon tagging category, the only track of that category used for tagging is the one with the largest value of θ_T , the CM angle between the track momentum and the missing D momentum. The tagging track must satisfy $\cos\theta_T < C_T$, where $C_T = 0.75$ ($C_T = 0.50$) for leptons (kaons), to minimize the impact of tracks originating from the D decay. If both a lepton and a kaon satisfy this requirement, the event is tagged with the lepton only.

We measure Δt using $\Delta t = (z_{\text{rec}} - z_{\text{tag}})/(\gamma\beta c)$, where z_{rec} (z_{tag}) is the decay position of the B_{rec} (B_{tag}) along the beam axis (z) in the laboratory frame, and the e^+e^- boost parameter $\gamma\beta$ is continuously calculated from the beam energies. To find z_{rec} , we use the π_h track parameters and errors, and the beam-spot position and size in the plane perpendicular to the beams (the $x - y$ plane). We find the position of the point in space for which the sum of the χ^2 contributions from the π_h track and the beam spot is a minimum. The z coordinate of this point determines z_{rec} . In lepton-tagged events, the same procedure, with the π_h track replaced by the tagging lepton, is used to determine z_{tag} .

In kaon-tagged events, we obtain z_{tag} from a beam-spot-constrained vertex fit of all tracks in the event, excluding π_h , π_s and all tracks within 1 rad of the D momentum in the CM frame. If the contribution of any track to the χ^2 of the vertex is more than 6, the track is removed and the fit is repeated until no track fails the $\chi^2 < 6$ requirement.

The Δt error $\sigma_{\Delta t}$ is calculated from the results of the z_{rec} and z_{tag} vertex fits.

3.4 PROBABILITY DENSITY FUNCTION

The analysis is carried out with a series of unbinned maximum-likelihood fits, performed simultaneously on the on- and off-resonance data samples and independently for the lepton-tagged and kaon-tagged events. The probability density function (PDF) depends on the variables m_{miss} , Δt , $\sigma_{\Delta t}$, F , s_t , and s_m , where F is a Fisher discriminant formed from fifteen event-shape variables that provide discrimination against continuum events [6], $s_t = 1$ (-1) when the B_{tag} is identified as a B^0 (\bar{B}^0), and $s_m = 1$ (-1) for “unmixed” (“mixed”) events. An event is labeled unmixed if the π_h is a π^- (π^+) and the B_{tag} is a B^0 (\bar{B}^0), and mixed otherwise.

The PDF for on-resonance data is a sum over the PDFs of the different event types:

$$P = \sum_i f_i P_i, \quad (3)$$

where the index $i = \{D^*\pi, D^*\rho, \text{peak}, \text{comb}, q\bar{q}\}$ indicates one of the event types described above, f_i is the relative fraction of events of type i in the data sample, and P_i is the PDF for these events. The PDF for off-resonance data is $P_{q\bar{q}}$. The parameter values for P_i are different for each event type, unless indicated otherwise. Each P_i is a product,

$$P_i = \mathcal{M}_i(m_{\text{miss}}) \mathcal{F}_i(F) T'_i(\Delta t, \sigma_{\Delta t}, s_t, s_m), \quad (4)$$

where the factors in Eq. (4) are described below.

3.4.1 m_{miss} AND F PDFs

The m_{miss} PDF for each event type i is the sum of a bifurcated Gaussian plus an ARGUS function:

$$\mathcal{M}_i(m_{\text{miss}}) = f_i^{\hat{\mathcal{G}}} \hat{\mathcal{G}}_i(m_{\text{miss}}) + (1 - f_i^{\hat{\mathcal{G}}}) \mathcal{A}_i(m_{\text{miss}}), \quad (5)$$

where $f_i^{\hat{\mathcal{G}}}$ is the bifurcated Gaussian fraction. The functions $\hat{\mathcal{G}}_i$ and \mathcal{A}_i are

$$\hat{\mathcal{G}}_i(x) \propto \begin{cases} \exp[-(x - M_i)^2/2\sigma_{Li}^2] & , \quad x < M_i \\ \exp[-(x - M_i)^2/2\sigma_{Ri}^2] & , \quad x > M_i \end{cases}, \quad (6)$$

$$\mathcal{A}(x) \propto \begin{cases} x \sqrt{1 - (x/M_i^A)^2} \exp\left[\epsilon_i \left(1 - (x/M_i^A)^2\right)\right] & , \quad x < M_i^A \\ 0 & , \quad x \geq M_i^A \end{cases}, \quad (7)$$

where M_i is the peak of the bifurcated Gaussian, σ_{Li} and σ_{Ri} are its left and right widths, ϵ_i is the ARGUS exponent, M_i^A is its end point, and the proportionality constants are such that each of these functions is normalized to unit area. The m_{miss} PDF of each event type has different parameter values.

The Fisher discriminant PDF \mathcal{F}_i for each event type is parameterized as a bifurcated Gaussian, as in Eq. (6). The parameter values of $\mathcal{F}_{D^*\pi}$, $\mathcal{F}_{D^*\rho}$, $\mathcal{F}_{\text{peak}}$, and $\mathcal{F}_{\text{comb}}$ are identical.

3.4.2 SIGNAL Δt PDFs

The Δt PDF $T'_{D^*\pi}(\Delta t, \sigma_{\Delta t}, s_t, s_m)$ for signal events corresponds to Eq. (1) with $O(r_{D^*\pi}^2)$ terms neglected, and with additional parameters that account for several experimental effects, described below.

The first effect has to do with the origin of the tagging track. In some of the events, the tagging track originates from the decay of the missing D . These events are labeled “missing- D tags” and do not provide any information regarding the flavor of the B_{tag} . In lepton tag events we further distinguish between “direct” tags, in which the tagging lepton originates directly from the decay of the B_{tag} , and “cascade” tags, where the tagging lepton is a daughter of a charmed particle produced in the B_{tag} decay. Cascade and direct tags have different mistag probabilities due to the different physical origin of the tagging track. In addition, the measured value of z_{tag} in cascade-lepton tags is systematically larger than the true value, due to the finite lifetime of the charmed particle and the boosted CM frame. This creates a correlation between the tag and vertex measurements that we address by considering cascade-lepton tags separately in the PDF⁶. In kaon tags, z_{tag} is determined using all available B_{tag} tracks. Therefore, the effect of the tagging track on the z_{tag} measurement is small, and no distinction between cascade and direct kaon tags is needed.

The second experimental effect is the finite detector resolution in the measurement of Δt . We address this by convoluting the distribution of the true decay time difference Δt_{tr} with a detector resolution function. Putting these two effects together, the Δt PDF of signal events is

$$T'_{D^*\pi}(\Delta t, \sigma_{\Delta t}, s_t, s_m) = (1 + \Delta\epsilon_{D^*\pi} s_t) \sum_j f_{D^*\pi}^j \int d\Delta t_{\text{tr}} T_{D^*\pi}^j(\Delta t_{\text{tr}}, s_t, s_m) \mathcal{R}_{D^*\pi}^j(\Delta t - \Delta t_{\text{tr}}, \sigma_{\Delta t}), \quad (8)$$

where $2\Delta\epsilon_{D^*\pi}$ is the relative difference between the detection efficiencies of positive and negative leptons or kaons, the index $j = \{\text{dir}, \text{cas}, \text{miss}\}$ indicates direct, cascade, and missing- D tags, and $f_{D^*\pi}^j$ is the fraction of signal events of tag-type j in the sample. We set $f_{D^*\pi}^{\text{dir}} = 1 - f_{D^*\pi}^{\text{cas}} - f_{D^*\pi}^{\text{miss}}$. For kaon tags $f_{D^*\pi}^{\text{cas}} = 0$. The function $T_{D^*\pi}^j(\Delta t_{\text{tr}}, s_t, s_m)$ is the Δt_{tr} distribution of tag-type j events, and $\mathcal{R}_{D^*\pi}^j(\Delta t - \Delta t_{\text{tr}}, \sigma_{\Delta t})$ is their resolution function, which parameterizes both the finite detector resolution and systematic offsets in the measurement of Δz , such as those due to the origin of the tagging particle. The parameterization of the resolution function is described in Sec. 3.4.4.

The Δt_{tr} PDF for missing- D tags is

$$T_{D^*\pi}^{\text{miss}}(\Delta t_{\text{tr}}, s_m) = \frac{e^{-|\Delta t_{\text{tr}}|/\tau_{D^*\pi}^{\text{miss}}}}{8\tau_{D^*\pi}^{\text{miss}}} \{1 + s_m (1 - 2\rho_{D^*\pi})\}, \quad (9)$$

where $\rho_{D^*\pi}$ is the probability that the charge of the tagging track is such that it results in a mixed flavor measurement.

The functional form of the direct and cascade tag Δt_{tr} PDFs is

$$T_{D^*\pi}^j(\Delta t_{\text{tr}}, s_t, s_m) = \frac{e^{-|\Delta t_{\text{tr}}|/\tau_{D^*\pi}}}{4\tau_{D^*\pi}} \left\{ 1 - s_t \Delta\omega_{D^*\pi}^j + s_m (1 - 2\omega_{D^*\pi}^j) \cos(\Delta m_{D^*\pi} \Delta t_{\text{tr}}) - \mathcal{S}_{D^*\pi}^j \sin(\Delta m_{D^*\pi} \Delta t_{\text{tr}}) \right\}, \quad (10)$$

where $j = \{\text{dir}, \text{cas}\}$, the mistag rate $\omega_{D^*\pi}^j$ is the probability to misidentify the flavor of the B_{tag} averaged over B^0 and \bar{B}^0 , and $\Delta\omega_{D^*\pi}^j$ is the B^0 mistag rate minus the \bar{B}^0 mistag rate. The factor $\mathcal{S}_{D^*\pi}^j$ describes CP violation due to interference between $b \rightarrow u\bar{c}d$ and $b \rightarrow c\bar{u}d$ amplitudes in both the B_{rec} and the B_{tag} decays:

$$\mathcal{S}_{D^*\pi}^j = (1 - 2\omega_{D^*\pi}^j) (s_t a_{D^*\pi} + s_m c_{D^*\pi}) + s_t s_m b_{D^*\pi} (1 - s_t \Delta\omega_{D^*\pi}^j), \quad (11)$$

⁶In Ref. [5] we corrected for the bias caused by this effect and included a systematic error due to its uncertainty.

where $a_{D^*\pi}$, $b_{D^*\pi}$, and $c_{D^*\pi}$ are related to the physical parameters through

$$\begin{aligned} a_{D^*\pi} &\equiv 2r_{D^*\pi} \sin(2\beta + \gamma) \cos \delta_{D^*\pi}, \\ b_{D^*\pi} &\equiv 2r' \sin(2\beta + \gamma) \cos \delta', \\ c_{D^*\pi} &\equiv 2 \cos(2\beta + \gamma)(r_{D^*\pi} \sin \delta_{D^*\pi} - r' \sin \delta'), \end{aligned} \quad (12)$$

and r' (δ') is the effective magnitude of the ratio of amplitudes (strong phase difference) between the $b \rightarrow u\bar{c}d$ and $b \rightarrow \bar{c}ud$ amplitudes in the B_{tag} decay. This parameterization is good to first order in $r_{D^*\pi}$ and r' . The inclusion of r' and δ' in the formalism accounts for cases where the B_{tag} undergoes a $b \rightarrow u\bar{c}d$ decay, and the kaon produced in the subsequent charm decay is used for tagging [7]. In lepton-tagged events $r' = 0$ (and hence $b_{D^*\pi} = 0$).

3.4.3 BACKGROUND Δt PDFs

The Δt PDF of $B \rightarrow D^{*\mp}\rho^\pm$ has the same functional form and parameter values as the signal PDF, except that the CP parameters $a_{D^*\rho}$, $b_{D^*\rho}$, and $c_{D^*\rho}$ are set to 0 and are later varied to evaluate systematic uncertainties. The validity of the use of the same non- CP parameters for $T'_{D^*\rho}$ and $T'_{D^*\pi}$ is established using simulated events, and stems from the fact that the π_h momentum spectrum in the $B \rightarrow D^{*\mp}\rho^\pm$ events that pass our selection criteria is almost identical to the signal spectrum.

The Δt PDF of the peaking background accounts separately for charged and neutral B decays:

$$\begin{aligned} T'_{\text{peak}}(\Delta t, \sigma_{\Delta t}, s_t, s_m) &= (1 + s_t \Delta\epsilon_{\text{peak}}) \\ &\times \left\{ T'^0_{\text{peak}} + \int d\Delta t_{\text{tr}} T'_{\text{peak}}^+(\Delta t_{\text{tr}}, s_t, s_m) \mathcal{R}^+_{\text{peak}}(\Delta t - \Delta t_{\text{tr}}, \sigma_{\Delta t}) \right\}, \end{aligned} \quad (13)$$

where T'^0_{peak} has the functional form of Eq. (8) and the subsequent expressions, Eqs. (9-12), but with all $D^*\pi$ -subscripted parameters replaced with their peak-subscripted counterparts. The integral in Eq. (13) accounts for the contribution of charged B decays to the peaking background, with

$$T'_{\text{peak}}^+(\Delta t_{\text{tr}}, s_t) = \frac{e^{-|\Delta t_{\text{tr}}|/\tau_{\text{peak}}^+}}{4\tau_{\text{peak}}^+} \left(1 - s_t \Delta\omega_{\text{peak}}^+\right), \quad (14)$$

and $\mathcal{R}^+_{\text{peak}}(\Delta t - \Delta t_{\text{tr}}, \sigma_{\Delta t})$ being the 3-Gaussian resolution function for these events.

Convergence of the fit with the parameterization of $T'_{D^*\pi}$ relies on our ability to independently determine $f_{D^*\pi}^{\text{miss}}$ using the angle between the π_s and the D^* , as described later in this note. That determination may not be carried out reliably for the combinatoric $B\bar{B}$ background, due to uncertainties in simulating the random nature of the reconstructed track combinations. As a result, the four parameters $f_{\text{comb}}^{\text{dir}}$, $\omega_{\text{comb}}^{\text{dir}}$, $\Delta\omega_{\text{comb}}^{\text{dir}}$, and ρ_{comb} are not independent, and can be reduced to the set of three parameters

$$\begin{aligned} \omega'_{\text{comb}} &= \omega_{\text{comb}}^{\text{dir}} (1 - f_{\text{comb}}^{\text{dir}}) + \frac{f_{\text{comb}}^{\text{dir}}}{2}, \\ \Delta\omega'_{\text{comb}} &= \Delta\omega_{\text{comb}} (1 - f_{\text{comb}}^{\text{dir}}), \\ \Omega_{\text{comb}} &= f_{\text{comb}}^{\text{dir}} (1 - 2\rho_{\text{comb}}). \end{aligned} \quad (15)$$

With these parameters and $f_{\text{comb}}^{\text{cas}} = 0$, the combinatoric $B\bar{B}$ background Δt PDF becomes

$$T'_{\text{comb}}(\Delta t, \sigma_{\Delta t}, s_t, s_m) = (1 + s_t \Delta\epsilon_{\text{comb}}) \int d\Delta t_{\text{tr}} T_{\text{comb}}(\Delta t_{\text{tr}}, s_t, s_m) \mathcal{R}_{\text{comb}}(\Delta t - \Delta t_{\text{tr}}, \sigma_{\Delta t}), \quad (16)$$

where $\mathcal{R}_{\text{comb}}(\Delta t - \Delta t_{\text{tr}}, \sigma_{\Delta t})$ is the 3-Gaussian resolution function and

$$T_{\text{comb}}(\Delta t_{\text{tr}}, s_t, s_m) = \frac{e^{-|\Delta t_{\text{tr}}|/\tau_{\text{comb}}}}{4\tau_{\text{comb}}} \left\{ \begin{aligned} &1 - s_t \Delta\omega'_{\text{comb}} + s_m \Omega_{\text{comb}} \\ &+ s_m (1 - 2\omega'_{\text{comb}}) \cos(\Delta m_{\text{comb}} \Delta t_{\text{tr}}) \\ &- \mathcal{S}_{\text{comb}} \sin(\Delta m_{\text{comb}} \Delta t_{\text{tr}}) \end{aligned} \right\}, \quad (17)$$

with

$$\mathcal{S}_{\text{comb}} = (1 - 2\omega'_{\text{comb}}) (s_t a_{\text{comb}} + s_m c_{\text{comb}}) + s_t s_m b_{\text{comb}} (1 - s_t \Delta\omega'_{\text{comb}}). \quad (18)$$

As in the case of $T_{D^*\rho}$, the CP parameters a_{peak} , b_{peak} , and c_{peak} are set to 0 and are later varied to evaluate systematic uncertainties. Parameters labeled with superscripts “peak” or “comb” are empirical and thus do not necessarily correspond to physical parameters and may have different values from those of the $D^*\pi$ -labeled parameters.

The PDF $T_{q\bar{q}}$ for the continuum background is the sum of two components, one with a finite lifetime and one with zero lifetime:

$$T'_{q\bar{q}}(\Delta t, \sigma_{\Delta t}, s_t) = (1 + s_t \Delta\epsilon_{q\bar{q}}) \int d\Delta t_{\text{tr}} T_{q\bar{q}}(\Delta t_{\text{tr}}, s_t, s_m) \mathcal{R}_{q\bar{q}}(\Delta t - \Delta t_{\text{tr}}, \sigma_{\Delta t}), \quad (19)$$

with

$$T_{q\bar{q}}(\Delta t_{\text{tr}}, s_t) = (1 - f_{q\bar{q}}^\delta) \frac{e^{-|\Delta t_{\text{tr}}|/\tau_{q\bar{q}}}}{4\tau_{q\bar{q}}} (1 - s_t \Delta\omega_{q\bar{q}}) + f_{q\bar{q}}^\delta \delta(\Delta t_{\text{tr}}), \quad (20)$$

where $f_{q\bar{q}}^\delta$ is the fraction of zero-lifetime events.

3.4.4 RESOLUTION FUNCTION PARAMETERIZATION

The resolution function for events of type i and optional secondary-type j ($j = \{\text{dir}, \text{cas}, \text{miss}\}$ for lepton-tagged signal events and $j = \{+, 0\}$ for the $B\bar{B}$ background types) is parameterized as the sum of three Gaussians:

$$\mathcal{R}_i^j(\Delta t - \Delta t_{\text{tr}}, \sigma_{\Delta t}) = f_i^{nj} \mathcal{G}_i^{nj}(t_r, \sigma_{\Delta t}) + (1 - f_i^{nj} - f_i^{oj}) \mathcal{G}_i^{wj}(t_r, \sigma_{\Delta t}) + f_i^{oj} \mathcal{G}_i^{oj}(t_r, \sigma_{\Delta t}), \quad (21)$$

where t_r is the residual $\Delta t - \Delta t_{\text{tr}}$, and \mathcal{G}_i^{nj} , \mathcal{G}_i^{wj} , and \mathcal{G}_i^{oj} are the “narrow”, “wide”, and “outlier” Gaussians. The narrow and wide Gaussians have the form

$$\mathcal{G}_i^{kj}(t_r, \sigma_{\Delta t}) \equiv \frac{1}{\sqrt{2\pi} s_i^{kj} \sigma_{\Delta t}} \exp\left(-\frac{(t_r - b_i^{kj} \sigma_{\Delta t})^2}{2(s_i^{kj} \sigma_{\Delta t})^2}\right), \quad (22)$$

where the index k takes the values $k = n, w$ for the narrow and wide Gaussians, and b_i^{kj} and s_i^{kj} are parameters determined by fits, as described in Sec. 3.5. The outlier Gaussian has the form

$$\mathcal{G}_i^{oj}(t_r, \sigma_{\Delta t}) \equiv \frac{1}{\sqrt{2\pi} s_i^{oj}} \exp\left(-\frac{(t_r - b_i^{oj})^2}{2(s_i^{oj})^2}\right), \quad (23)$$

where in all nominal fits the values of b_i^{oj} and s_i^{oj} are fixed to 0 ps and 8 ps, respectively, and are later varied to evaluate systematic errors.

3.5 ANALYSIS PROCEDURE

The analysis proceeds in four steps involving unbinned maximum likelihood fits to the data:

1. In the first step, we determine the parameters $f_{D^*\rho} + f_{D^*\pi}$, f_{peak} , and f_{comb} of Eq. (3). In order to reduce the reliance on the simulation, we also obtain in the same fit the parameters $f_{q\bar{q}}^{\hat{G}}$ of Eq. (5), $\epsilon_{q\bar{q}}$ of Eq. (7), σ_L for the signal (Eq. 6) and all the parameters of $\mathcal{F}_{q\bar{q}}$, and $\mathcal{F}_{B\bar{B}}$ (the latter applies to all $B\bar{B}$ event types). This is done by fitting the data with the PDF

$$P_i = \mathcal{M}_i(m_{\text{miss}}) \mathcal{F}_i(F), \quad (24)$$

instead of Eq. (4), i.e. by ignoring the time dependence. The fraction $f_{q\bar{q}}$ of continuum events is determined from the event yield of the off-resonance sample and its integrated luminosity relative to the on-resonance sample. All other parameters of the \mathcal{M}_i PDFs and the value of $f_{D^*\pi}/(f_{D^*\pi} + f_{D^*\rho})$ are obtained from the MC simulation.

2. In the second step, we repeat the fit of the first step for data events with $\cos\theta_T \geq C_T$, to obtain the fraction of signal events in that sample. Given this fraction and the relative efficiencies for direct, cascade, and missing- D signal events to satisfy the $\cos\theta_T < C_T$ requirement, we calculate $f_{D^*\pi}^{\text{miss}}$. We also calculate the value of $\rho_{D^*\pi}$ from the fractions of mixed and unmixed signal events in the $\cos\theta_T \geq C_T$ sample relative to the $\cos\theta_T < C_T$ sample.
3. In the third step, we fit the data events in the sideband $1.81 < m_{\text{miss}} < 1.84$ GeV/ c^2 with the 3-dimensional PDFs of Eq. (4). The parameters of $\mathcal{M}_i(m_{\text{miss}})$ and $\mathcal{F}_i(F)$, and the fractions f_i are fixed to the values obtained in the first step. From this fit we obtain the parameters of T'_{comb} , as well as those of $T'_{q\bar{q}}$.
4. In the fourth step, we fix all the parameter values obtained in the previous steps and fit the events in the signal region $1.845 < m_{\text{miss}} < 1.880$ GeV/ c^2 , determining the parameters of $T'_{D^*\pi}$ and $T'_{q\bar{q}}$. Simulation studies show that the parameters of T'_{comb} are independent of m_{miss} , enabling us to obtain them in the sideband fit (step 3) and then use them in the signal-region fit. The same is not true of the $T'_{q\bar{q}}$ parameters; hence they are free parameters in the signal-region fit of the last step.

4 RESULTS

The fit of step 1 finds 16060 ± 210 signal $B^0 \rightarrow D^{*\mp}\pi^{\pm}$ events in the lepton-tag category and 57480 ± 540 in the kaon-tag category. The m_{miss} and F distributions for data are shown in Figs. 1 and 2, with the PDFs overlaid.

The results of the signal region fit for lepton-tagged events are summarized in Table 1, and the plots of the Δt distributions for the data are shown in Fig. 3. Results of the fit for the kaon-tagged events are shown in Table 2 and Fig. 4. For each of the plots in this figure we calculate the Kolmogorov-Smirnov probabilities for the PDF and data to originate from the same distribution, as a way to verify the goodness of the fit. The probabilities are 41%, 99%, 99%, and 26%. Fig. 5 shows the raw, time-dependent CP asymmetry

$$A(\Delta t) = \frac{N_{s_t=1}(\Delta t) - N_{s_t=-1}(\Delta t)}{N_{s_t=1}(\Delta t) + N_{s_t=-1}(\Delta t)}. \quad (25)$$

In the absence of background and with high statistics, perfect tagging, and perfect Δt measurement, $A(\Delta t)$ would be a sinusoidal oscillation with amplitude $a_{D^*\pi}$.

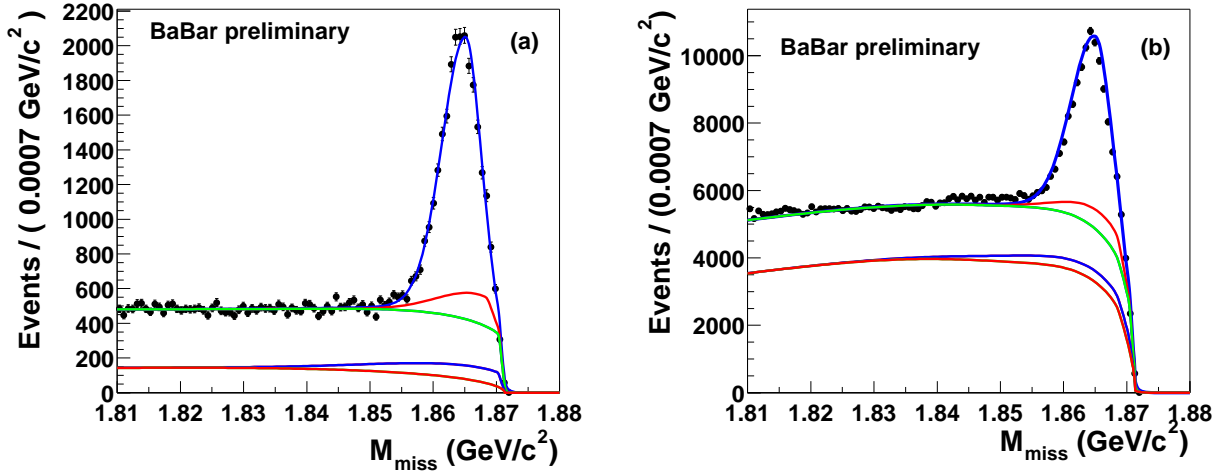


Figure 1: The m_{miss} distributions for on-resonance lepton-tagged (left) and kaon-tagged (right) data. The curves show, from bottom to top, the cumulative contributions of the continuum, peaking $B\bar{B}$, combinatoric $B\bar{B}$, $B \rightarrow D^{*\mp}\rho^\pm$, and $B^0 \rightarrow D^{*\mp}\pi^\pm$ PDF components.

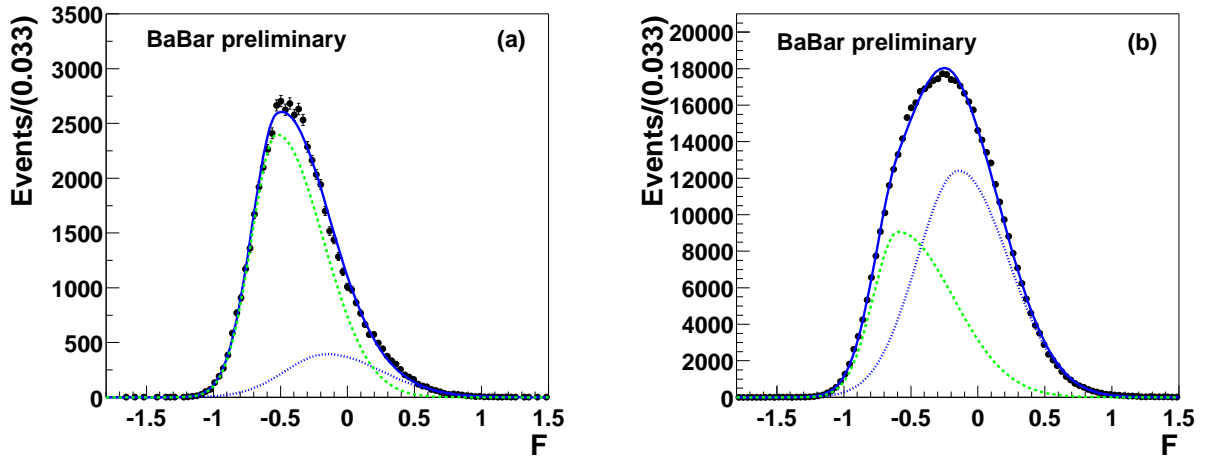


Figure 2: The F distributions for on-resonance lepton-tagged (left) and kaon-tagged (right) data. The contributions of the $B\bar{B}$ (dashed line) and the continuum (dot line) PDF components are overlaid, peaking at approximately -0.6 and -0.1 , respectively. Also overlaid is the total PDF.

Parameter		Value
signal		
$2r_{D^*\pi} \sin(2\beta + \gamma) \cos \delta_{D^*\pi}$	$a_{D^*\pi}^\ell$	-0.048 ± 0.022
$2r_{D^*\pi} \cos(2\beta + \gamma) \sin \delta_{D^*\pi}$	$c_{D^*\pi}^\ell$	-0.015 ± 0.036
$B^0 - \bar{B}^0$ mixing frequency	$\Delta m_{D^*\pi}$	$0.537 \pm 0.011 \text{ ps}^{-1}$
B^0 lifetime	$\tau_{D^*\pi}$	$1.435 \pm 0.019 \text{ ps}$
mistag (direct tags)	$\omega_{D^*\pi}^{\text{dir}}$	0.008 ± 0.003
bias of \mathcal{G}_{cas}^n	$b_{D^*\pi}^{n \text{ cas}}$	-0.43 ± 0.22
bias of \mathcal{G}_{dir}^n	$b_{D^*\pi}^{n \text{ dir}}$	0.000 ± 0.034
bias of \mathcal{G}_{dir}^w	$b_{D^*\pi}^{w \text{ dir}}$	0.04 ± 0.40
fraction of \mathcal{G}_{dir}^n	$f_{D^*\pi}^{n \text{ dir}}$	0.918 ± 0.065
fraction of \mathcal{G}_{dir}^o	$f_{D^*\pi}^{o \text{ dir}}$	0.005 ± 0.005
width of \mathcal{G}_{dir}^n	$s_{D^*\pi}^{n \text{ dir}}$	1.047 ± 0.063
width of \mathcal{G}_{dir}^w	$s_{D^*\pi}^{w \text{ dir}}$	2.43 ± 0.68
continuum		
$q\bar{q}$ effective lifetime	$\tau_{q\bar{q}}$	$1.12 \pm 0.22 \text{ ps}$
mistag	$\omega_{q\bar{q}}$	0.343 ± 0.011
mistag difference	$\Delta\omega_{q\bar{q}}$	-0.095 ± 0.022
fraction of 0-lifetime events	$f_{q\bar{q}}^\delta$	0.775 ± 0.037
bias of \mathcal{G}^n	$b_{q\bar{q}}^n$	0.047 ± 0.054
bias of \mathcal{G}^w	$b_{q\bar{q}}^w$	-1.73 ± 0.83
fraction of \mathcal{G}^n	$f_{q\bar{q}}^n$	0.848 ± 0.055
fraction of \mathcal{G}^o	$f_{q\bar{q}}^o$	0.072 ± 0.015
width of \mathcal{G}^n	$s_{q\bar{q}}^n$	0.982 ± 0.052

Table 1: Results of the fit of the lepton-tagged events in the signal region $1.845 < m_{\text{miss}} < 1.880 \text{ GeV}/c^2$. Errors are statistical only.

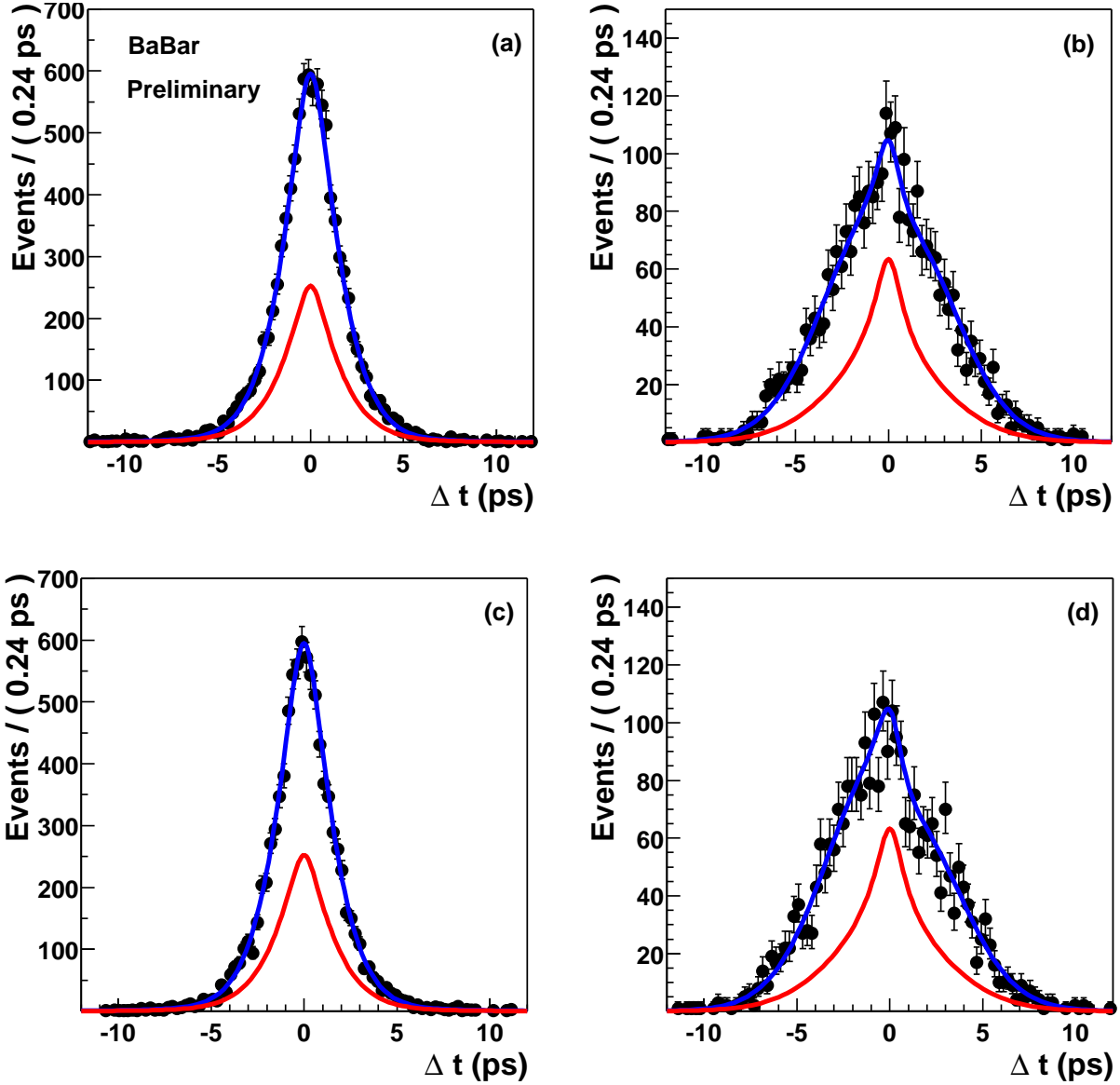


Figure 3: Δt distributions for the lepton-tagged events separated according to the tagged flavor of B_{tag} and whether they were found to be mixed or unmixed: a) B^0 unmixed b) B^0 mixed c) \bar{B}^0 unmixed, d) \bar{B}^0 mixed. The curves show the PDF, calculated with the parameters obtained by the fit. Also shown is the PDF of the total background. The requirements $m_{\text{miss}} > 1.855 \text{ GeV}/c^2$, $F < 0$ are applied in order to reduce the background.

Parameter		Value
signal		
$2r_{D^*\pi} \sin(2\beta + \gamma) \cos \delta_{D^*\pi}$	$a_{D^*\pi}^K$	-0.033 ± 0.023
$2r' \sin(2\beta + \gamma) \cos \delta'$	$b_{D^*\pi}^K$	-0.004 ± 0.012
$2 \cos(2\beta + \gamma)(r_{D^*\pi} \sin \delta_{D^*\pi} - r' \sin \delta')$	$c_{D^*\pi}^K$	0.019 ± 0.023
$B^0 - \bar{B}^0$ mixing frequency	$\Delta m_{D^*\pi}$	$0.4716 \pm 0.0087 \text{ ps}^{-1}$
B^0 effective lifetime	$\tau_{D^*\pi}$	$1.379 \pm 0.012 \text{ ps}$
mistag	$\omega_{D^*\pi}$	0.226 ± 0.0036
mistag difference	$\Delta \omega_{D^*\pi}$	-0.0301 ± 0.0052
efficiency difference	$\Delta \epsilon_{D^*\pi}$	-0.0126 ± 0.0055
bias of \mathcal{G}^n	$b_{D^*\pi}^n$	-0.287 ± 0.022
bias of \mathcal{G}^w	$b_{D^*\pi}^w$	0.044 ± 0.067
fraction of \mathcal{G}^n	$f_{D^*\pi}^n$	0.909 ± 0.040
fraction of \mathcal{G}^o	$f_{D^*\pi}^o$	0.014 ± 0.002
width of \mathcal{G}^n	$s_{D^*\pi}^n$	1.109 ± 0.039
width of \mathcal{G}^w	$s_{D^*\pi}^w$	0.01 ± 0.23
continuum		
$q\bar{q}$ effective lifetime	$\tau_{q\bar{q}}$	$0.546 \pm 0.037 \text{ ps}$
mistag of non-0-lifetime events	$\omega_{q\bar{q}}^\tau$	0.000 ± 0.002
mistag of 0-lifetime events	$\omega_{q\bar{q}}^\delta$	0.334 ± 0.010
fraction of 0-lifetime events	$f_{q\bar{q}}^\delta$	0.768 ± 0.021
bias of \mathcal{G}^n	$b_{q\bar{q}}^n$	0.013 ± 0.007
bias of \mathcal{G}^w	$b_{q\bar{q}}^w$	0.130 ± 0.047
fraction of \mathcal{G}^n	$f_{q\bar{q}}^n$	0.853 ± 0.026
fraction of \mathcal{G}^o	$f_{q\bar{q}}^o$	0.013 ± 0.001
width of \mathcal{G}^n	$s_{q\bar{q}}^n$	1.029 ± 0.013
width of \mathcal{G}^w	$s_{q\bar{q}}^w$	1.90 ± 0.11

Table 2: Results of the fit of the kaon-tagged events in the signal region $1.845 < m_{\text{miss}} < 1.880 \text{ GeV}/c^2$. Errors are statistical only.

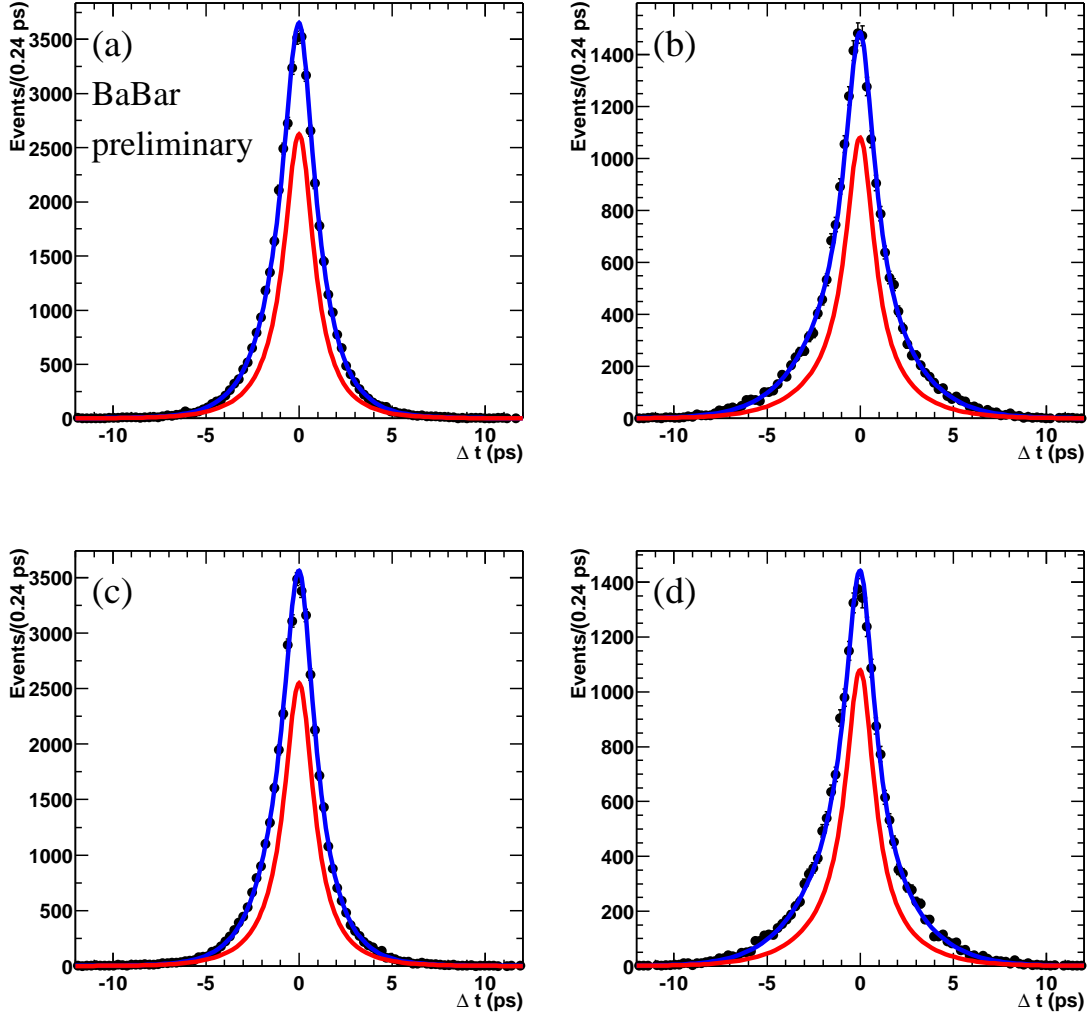


Figure 4: Δt distributions for the kaon-tagged events separated according to the tagged flavor of B_{tag} and whether they were found to be mixed or unmixed: a) B^0 unmixed b) B^0 mixed c) \bar{B}^0 unmixed, d) \bar{B}^0 mixed. The curves show the PDF, calculated with the parameters obtained by the fit. Also shown is the PDF of the total background. The requirements $m_{\text{miss}} > 1.855 \text{ GeV}/c^2$, $F < 0$ are applied in order to reduce the background.

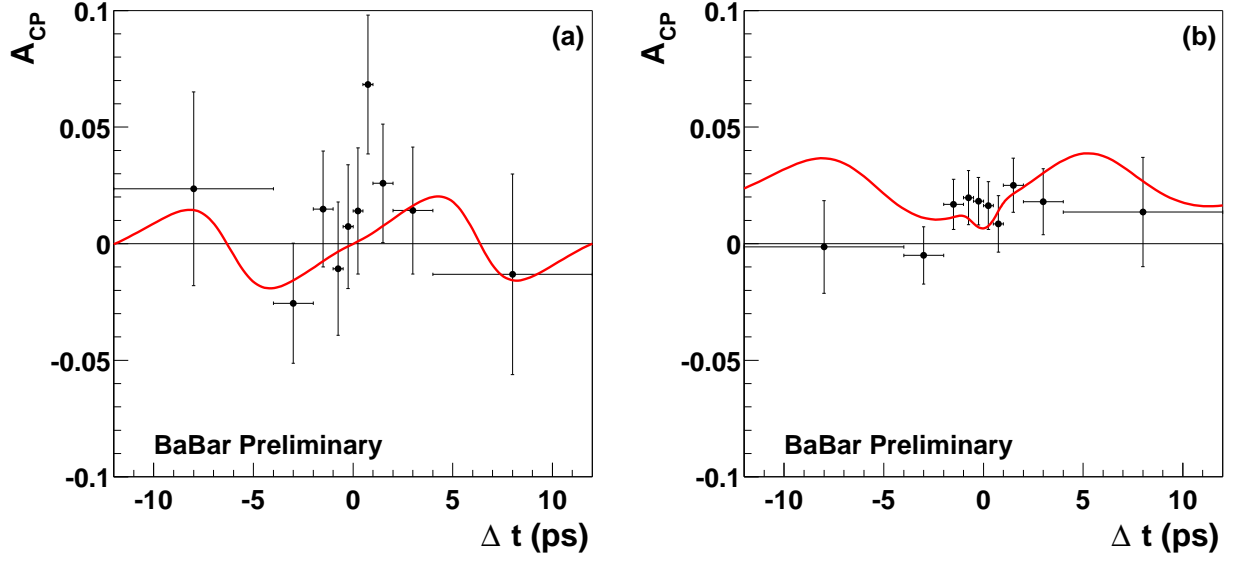


Figure 5: Raw asymmetry for (a) lepton-tagged and (b) kaon-tagged events. The curve represents the projection of the PDF for the raw asymmetry. The requirements $m_{\text{miss}} > 1.855 \text{ GeV}/c^2$, $F < 0$ are applied in order to reduce the background. A non-zero value of $a_{D^*\pi}$ would show up as a sinusoidal asymmetry, up to resolution and background effects. The offset from the horizontal axis in the kaon-tag plot is due to the nonzero value of $\Delta\epsilon_{D^*\pi}$.

Source	Error ($\times 10^{-2}$)	
	$a_{D^*\pi}^\ell$	$c_{D^*\pi}^\ell$
1. Step 1 fit	0.04	0.04
2. Sideband statistics	0.08	0.08
3. $f_{D^*\pi}^{\text{miss}}$	0.02	0.02
4. ρ	0.02	0.02
5. MC statistics	0.6	1.2
6. Beam spot size	0.10	0.10
7. Detector z scale	0.03	0.03
8. Detector alignment	0.4	0.8
9. Combinatoric background CP content	0.25	0.22
10. Peaking background CP content	0.36	0.38
11. $D^*\rho$ CP content	0.53	0.52
12. Peaking background	0.21	0.31
13. Signal region/sideband difference	0.0003	0.002
14. $\mathcal{B}(B \rightarrow D^{*\mp}\rho^\pm)$	0.17	0.33
15. Variation of $\tau_{D^*\pi}$ and $\Delta m_{D^*\pi}$	0.21	0.95
Total systematic error	1.04	1.89
Statistical uncertainty	2.2	3.6

Table 3: Systematic errors in $a_{D^*\pi}^\ell$ and $c_{D^*\pi}^\ell$ for lepton-tagged events.

5 SYSTEMATIC STUDIES

The systematic errors are summarized in Tables 3 and 4 for lepton- and kaon-tagged events, respectively. Each item below corresponds to the item with the same number in Tables 3 and 4.

1. The statistical errors from the fit in Step 1 are propagated to the final fit, taking their correlations into account. It also includes the systematic errors due to possible differences between the PDF line shape and the data points in the kinematical fit.
2. The statistical errors from the m_{miss} sideband fit (Step 3) are propagated to the final fit (Step 4), taking their correlations into account.
- 3-4. The statistical errors from the Step 2 fits are propagated to the final fit.
5. The statistical errors associated with all the parameters obtained from MC are propagated to the final fit.
6. The effect of uncertainties in the beam-spot size on the vertex constraint is estimated by increasing the beam spot size by $50 \mu\text{m}$.
7. The effect of the uncertainty in the measured length of the detector in the z direction is evaluated by applying a 0.6% variation to the measured values of Δt and $\sigma_{\Delta t}$.
8. To evaluate the effect of possible misalignments in the SVT, signal MC events are reconstructed with different alignment parameters, and the analysis is repeated.

Source	Error ($\times 10^{-2}$)		
	$a_{D^*\pi}^K$	$b_{D^*\pi}^K$	$c_{D^*\pi}^K$
1. Step 1 fit	0.10	0.04	0.04
2. Sideband statistics	0.40	0.12	0.44
3. $f_{D^*\pi}^{\text{miss}}$	0.02	negl.	negl.
4. ρ	0.02	negl.	negl.
5. MC statistics	0.8	0.4	0.9
6. Beam spot size	0.07	0.13	0.06
7. Detector z scale	0.02	negl.	0.03
8. Detector alignment	0.41	0.14	0.74
9. Combinatoric background CP content	0.80	0.56	0.72
10. Peaking background CP content	0.29	0.17	0.27
11. $D^*\rho$ CP content	0.57	0.58	0.58
12. Peaking background	0.21	0.41	0.31
13. Signal region/sideband difference	0.04	0.03	0.05
14. $\mathcal{B}(B \rightarrow D^{*\mp}\rho^\pm)$	0.17	0.22	0.33
15. Variation of $\tau_{D^*\pi}$ and $\Delta m_{D^*\pi}$	0.26	0.16	0.05
Total systematic error	1.47	1.06	1.63
Statistical uncertainty	2.3	1.2	2.3

Table 4: Systematic errors in $a_{D^*\pi}^K$, $b_{D^*\pi}^K$, and $c_{D^*\pi}^K$ for kaon-tagged events.

- 9-11. The CP parameters of the $B \rightarrow D^{*\mp}\rho^\pm$, peaking, and combinatoric $B\bar{B}$ background are fixed to 0 in the fits. To study the effect of possible CP violation in these backgrounds, their CP parameters are varied in the range ± 0.04 and the step-4 fit is repeated.
12. The uncertainty due to the parameters of T'_{peak} is evaluated by fitting the simulated sample, setting the parameters of T'_{peak} to be identical to those of T'_{comb} .
13. The uncertainty due to possible differences between the Δt distributions for the combinatoric background in the m_{miss} sideband and signal region is evaluated by comparing the results of fitting the simulated sample with the T'_{comb} parameters taken from the sideband or the signal region.
14. The ratio $f_{D^*\rho}/f_{D^*\pi}$ is varied by the uncertainty in the corresponding ratio of branching fractions, obtained from Ref. [10].
15. The lifetime and mixing parameters from the fits are not very consistent with the world average values when only the statistical uncertainties from the fit are considered. However, the inconsistency is significantly reduced when the estimated systematic uncertainties on the $\tau_{D^*\pi}$ and $\Delta m_{D^*\pi}$ parameters are included. To determine the systematic errors on the CP parameters due to $\tau_{D^*\pi}$ and $\Delta m_{D^*\pi}$, we repeat the fit with these parameters fixed to their world-average values from Ref. [10]. Because of the small correlations between these parameters and the CP parameters ($\leq 2\%$ for the kaon-tagged sample and $\leq 9\%$ for the lepton-tagged sample), the resulting changes in the CP parameters are small. These changes are assigned as systematic uncertainties.

6 PHYSICS RESULTS

Summarizing the values and uncertainties of the CP parameters, we obtain the following results from the lepton-tagged sample:

$$\begin{aligned} a_{D^*\pi}^\ell &= 2r_{D^*\pi} \sin(2\beta + \gamma) \cos \delta_{D^*\pi} = -0.048 \pm 0.022 \pm 0.010, \\ c_{D^*\pi}^\ell &= 2r_{D^*\pi} \cos(2\beta + \gamma) \sin \delta_{D^*\pi} = -0.015 \pm 0.036 \pm 0.019. \end{aligned} \quad (26)$$

The results from the kaon-tagged sample fits are

$$\begin{aligned} a_{D^*\pi}^K &= 2r_{D^*\pi} \sin(2\beta + \gamma) \cos \delta_{D^*\pi} = -0.033 \pm 0.023 \pm 0.015, \\ b_{D^*\pi}^K &= 2r' \sin(2\beta + \gamma) \cos \delta' = -0.004 \pm 0.012 \pm 0.011, \\ c_{D^*\pi}^K &= 2 \cos(2\beta + \gamma)(r_{D^*\pi} \sin \delta_{D^*\pi} - r' \sin \delta') = +0.019 \pm 0.023 \pm 0.016. \end{aligned} \quad (27)$$

Combining the results for lepton and kaon tags gives the amplitude of the time-dependent CP asymmetry,

$$a_{D^*\pi} = 2r_{D^*\pi} \sin(2\beta + \gamma) \cos \delta_{D^*\pi} = -0.041 \pm 0.016 \text{ (stat.)} \pm 0.010 \text{ (syst.)}, \quad (28)$$

where the systematic error takes into account correlations between the individual results. This result deviates from zero by 2.2 standard deviations.

We use two methods for interpreting our results in terms of constraints on $|\sin(2\beta + \gamma)|$. Both methods involve minimizing a χ^2 function that is symmetric under the exchange $\sin(2\beta + \gamma) \rightarrow -\sin(2\beta + \gamma)$, and applying the method of Ref. [11]. In the first method we make no assumption regarding the value of $r_{D^*\pi}$. For different values of $r_{D^*\pi}$, we vary $\delta_{D^*\pi}$ and $\sin(2\beta + \gamma)$ so as to minimize the function

$$\chi^2(r_{D^*\pi}, \sin(2\beta + \gamma), \delta_{D^*\pi}) = \sum_{j,k=1}^3 \Delta x_j V_{jk}^{-1} \Delta x_k, \quad (29)$$

where Δx_j refers to the difference between the result of our measurement of $a_{D^*\pi}^K$, $a_{D^*\pi}^\ell$, or $c_{D^*\pi}^\ell$ (Eqs. (27) and (26)) and the theoretical expressions given by Eq. (12). The measurements of $b_{D^*\pi}^K$ and $c_{D^*\pi}^K$ are not used in the fit, since they depend on the unknown values of r' and δ' . The measurement error matrix V is nearly diagonal, and accounts for correlations between the measurements due to correlated statistical and systematic uncertainties. The parameters determined by this fit are $\sin(2\beta + \gamma)$, which is limited to lie in the range $[-1, 1]$, and $\delta_{D^*\pi}$. We then generate many parameterized MC experiments with the same sensitivity as reported here for different values of $\sin(2\beta + \gamma)$ and with $\delta_{D^*\pi} = 0$, which yields the most conservative lower limit on $|\sin(2\beta + \gamma)|$. The fraction of these experiments in which $\chi^2(\sin(2\beta + \gamma)) - \chi_{\min}^2$ is smaller than in the data is interpreted as the confidence level (CL) of the limit on $|\sin(2\beta + \gamma)|$. The resulting 90% CL lower limit on $|\sin(2\beta + \gamma)|$ is shown as a function of $r_{D^*\pi}$ in Fig. 6. This limit is always based on the more conservative of the two possibilities implied by the ambiguity $|\sin(2\beta + \gamma)| \leftrightarrow |\cos \delta_{D^*\pi}|$.

The second method assumes that $r_{D^*\pi}$ can be estimated from the Cabibbo angle, the ratio of branching fractions $\mathcal{B}(B^0 \rightarrow D_s^{*+} \pi^-) / \mathcal{B}(B^0 \rightarrow D_s^{*-} \pi^+)$ [12], and the ratio of decay constants $f_{D^*} / f_{D_s^*}$ [13], yielding the measured value

$$r_{D^*\pi}^{\text{meas}} = 0.015_{-0.006}^{+0.004}. \quad (30)$$

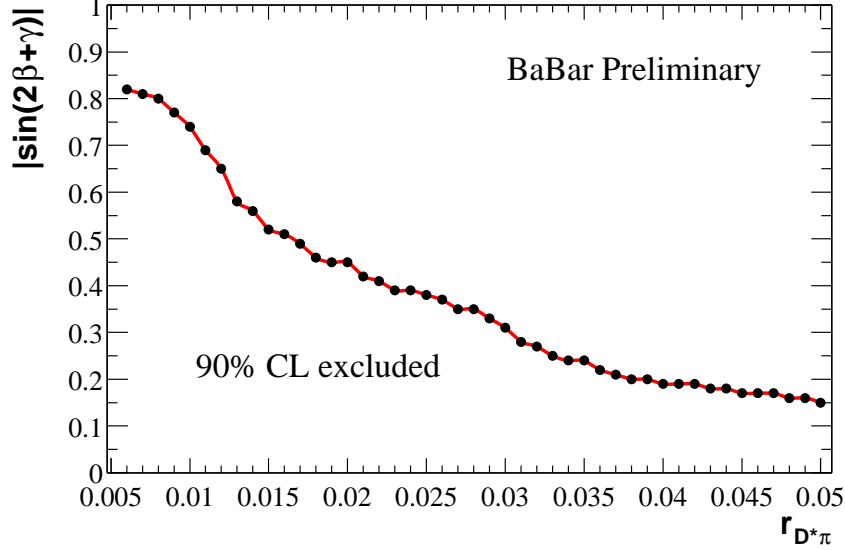


Figure 6: Lower limit on $|\sin(2\beta + \gamma)|$ at 90% CL as a function of $r_{D^*\pi}$.

This value includes our recent measurement of the branching fraction $B(D_s^+ \rightarrow \phi\pi^+)$ [14]. In addition to the above experimental errors, we attribute a non-Gaussian 30% relative error to the theoretical assumptions involved in obtaining this value. To obtain the limits with these assumptions, we minimize the function

$$\tilde{\chi}^2 = \chi^2 + \Delta^2(r_{D^*\pi}), \quad (31)$$

where the term $\Delta^2(r_{D^*\pi})$ takes into account both the Gaussian experimental errors of Eq. (30) and the 30% theoretical uncertainty [15]:

$$\Delta^2(r_{D^*\pi}) = \begin{cases} \left(\frac{r_{D^*\pi} - 1.3 r_{D^*\pi}^{\text{meas}}}{0.005} \right)^2, & \xi_{r_{D^*\pi}} > 0.3 \\ 0, & |\xi_{r_{D^*\pi}}| \leq 0.3 \\ \left(\frac{r_{D^*\pi} - 0.7 r_{D^*\pi}^{\text{meas}}}{0.007} \right)^2, & \xi_{r_{D^*\pi}} < -0.3 \end{cases}, \quad (32)$$

where $\xi_{r_{D^*\pi}} \equiv (r_{D^*\pi} - r_{D^*\pi}^{\text{meas}})/r_{D^*\pi}^{\text{meas}}$. The parameters

$$\begin{aligned} \sin(2\beta + \gamma) &= 0.97 \pm 1.22, \\ \delta_{D^*\pi} &= 0.24 \pm 1.23, \\ r_{D^*\pi} &= 0.020 \pm 0.004 \end{aligned} \quad (33)$$

are determined in this fit. Due to the fact that the minimum value occurs close to the boundary of the physical region ($|\sin(2\beta + \gamma)| = 1$), the errors in Eq. 33 are not relevant and in order to give a probabilistic interpretation the method of Ref. [11] has been used. The resulting confidence level as a function of the lower limit on $|\sin(2\beta + \gamma)|$, evaluated using parameterized MC experiments as in the first method, is shown in Fig. 7. In particular, we find the limits $|\sin(2\beta + \gamma)| > 0.75$ (0.58) at 68% (90%) CL. The implied contours of constant probability for the apex of the unitary triangle appear in Fig. 8.

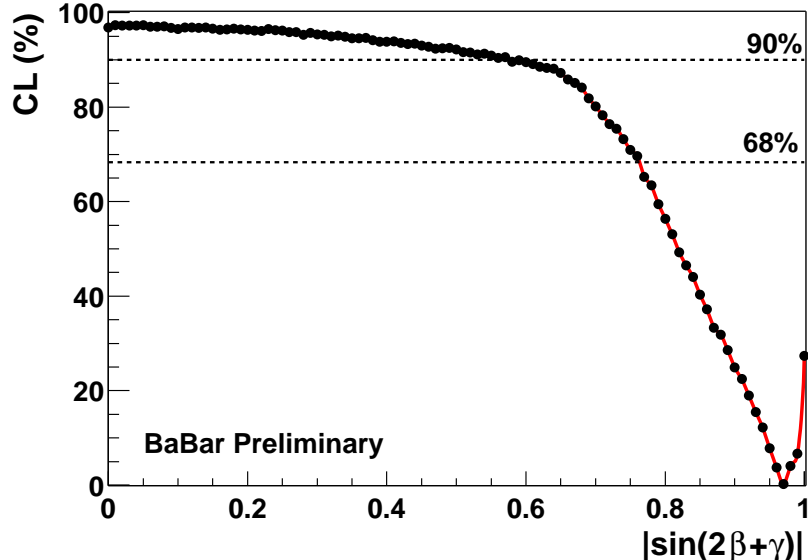


Figure 7: Confidence level as a function of the lower limit on $|\sin(2\beta + \gamma)|$ given $r_{D^*\pi}$ from Eq. (30).

7 SUMMARY

We present a preliminary measurement of the time-dependent CP asymmetry and parameters related to $\sin(2\beta + \gamma)$ in a sample of partially reconstructed $B^0 \rightarrow D^{*+}\pi^-$ events. In particular, the amplitude of the measured asymmetry is

$$a_{D^*\pi} = 2r_{D^*\pi} \sin(2\beta + \gamma) \cos \delta_{D^*\pi} = -0.041 \pm 0.016 \text{ (stat.)} \pm 0.010 \text{ (syst.)}. \quad (34)$$

We interpret our results in terms of the lower limits $|\sin(2\beta + \gamma)| > 0.75$ (0.58) at 68% (90%) CL, and extract limits as a function of the ratio $r_{D^*\pi}$ between the $b \rightarrow u\bar{c}d$ and $b \rightarrow \bar{c}u d$ decay amplitudes.

8 ACKNOWLEDGMENTS

We are grateful for the extraordinary contributions of our PEP-II colleagues in achieving the excellent luminosity and machine conditions that have made this work possible. The success of this project also relies critically on the expertise and dedication of the computing organizations that support *BABAR*. The collaborating institutions wish to thank SLAC for its support and the kind hospitality extended to them. This work is supported by the US Department of Energy and National Science Foundation, the Natural Sciences and Engineering Research Council (Canada), Institute of High Energy Physics (China), the Commissariat à l’Energie Atomique and Institut National de Physique Nucléaire et de Physique des Particules (France), the Bundesministerium für Bildung und Forschung and Deutsche Forschungsgemeinschaft (Germany), the Istituto Nazionale di Fisica Nucleare (Italy), the Foundation for Fundamental Research on Matter (The Netherlands), the Research Council of Norway, the Ministry of Science and Technology of the Russian Federation, and the Particle Physics and Astronomy Research Council (United Kingdom). Individuals have received support from CONACyT (Mexico), the A. P. Sloan Foundation, the Research Corporation, and the Alexander von Humboldt Foundation.

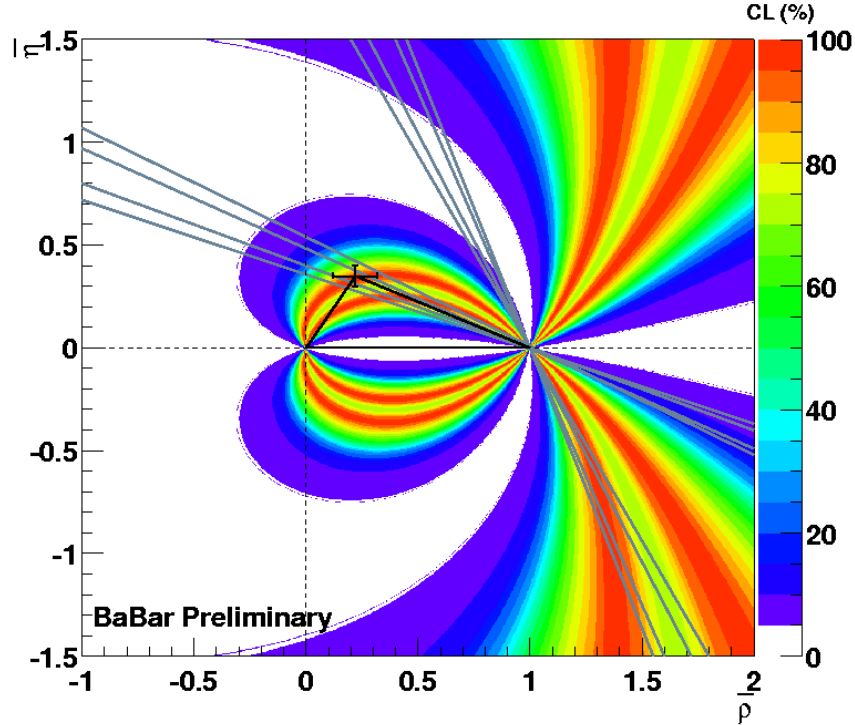


Figure 8: Contours of constant probability (color-coded in percent) for the position of the apex of the unitarity triangle to be inside the contour, based on the results of Fig. 7. The one- and two-standard deviation ranges of the world average $\sin 2\beta$ measurement ($\sin 2\beta = 0.736 \pm 0.049$) are shown as gray lines. The cross represents the value and errors of the apex of the unitarity triangle from the standard CKMFitter fit [16].

References

- [1] N. Cabibbo, Phys. Rev. Lett. **10**, 531 (1963); M. Kobayashi and T. Maskawa, Prog. Theoret. Phys. **49**, 652 (1973).
- [2] I. Dunietz, Phys. Lett. B **427**, 179 (1998).
- [3] BABAR Collaboration, B. Aubert *et al.*, Phys. Rev. Lett. **89**, 201802 (2002); Belle Collaboration, K. Abe *et al.*, Phys. Rev. D **66**, 071102 (2002).
- [4] L. Wolfenstein, Phys. Rev. Lett. **51**, 1945 (1983).
- [5] BABAR Collaboration, B. Aubert *et al.*, Phys. Rev. Lett. **92**, 251802 (2004).
- [6] BABAR Collaboration, B. Aubert *et al.*, Phys. Rev. D **67**, 091101 (2003).
- [7] O. Long, M. Baak, R.N. Cahn and D. Kirkby, Phys. Rev. D **68**, 034010 (2003).
- [8] BABAR Collaboration, B. Aubert *et al.*, Nucl. Instrum. Methods A **479**, 1 (2002).
- [9] Particle Data Group, K. Hagiwara *et al.*, Phys. Rev. D **66**, 010001 (2002).

- [10] Particle Data Group, S. Eidelman *et al.*, Phys. Lett. B **592**, 1 (2004).
- [11] G. Feldman and R. Cousins, Phys. Rev. D **57**, 3873 (1998).
- [12] Belle Collaboration, P. Krokovny *et al.*, Phys. Rev. Lett. **89**, 231804 (2002); *BABAR* Collaboration, B. Aubert *et al.*, Phys. Rev. Lett. **90**, 181803 (2003).
- [13] D. Becirevic, Nucl. Phys. Proc. Suppl. **94**, 337 (2001).
- [14] *BABAR* Collaboration, B. Aubert *et al.*, “Partial Reconstruction of $B^0 \rightarrow D_s^{*+} D^{*-}$ Decays and Measurement of the $D_s^+ \rightarrow \phi\pi^+$ Branching Fraction”, submitted to the 32nd International Conference on High-Energy Physics, ICHEP 04, 16 August—22 August 2004, Beijing, China.
- [15] A. Höcker *et al.*, Eur. Phys. J. C **21**, 225 (2001).
- [16] <http://ckmfitter.in2p3.fr/>